A Doppler De-aliasing Technique for FMCW-TDM MIMO Automotive Radar

Yuan, S.; Dash, T.K.; Roldan Montero, I.; Fioranelli, F.; Yarovoy, Alexander

DOI
10.1109/TIM.2025.3623765

Publication date
2025

Document Version
Final published version

Published in
IEEE Transactions on Instrumentation and Measurement

A Doppler De-Aliasing Technique for FMCW-TDM MIMO Automotive Radar

Sen Yuan, *Member, IEEE*, Tworit Dash, *Member, IEEE*, Ignacio Roldan, Francesco Fioranelli, *Senior Member, IEEE*, and Alexander G. Yarovoy, *Fellow, IEEE*

***Abstract*—The problem of diminished unambiguous target velocity interval induced by the time-division-multiplex mode (TDM) of multiple-input–multiple-output (MIMO) frequency-modulated continuous-wave (FMCW) automotive radar has been explored. A novel MIMO antenna array activation mode and a parametric approach for Doppler de-aliasing based on a two-step cross-entropy optimization are proposed. The TDM Doppler signal model has been derived, and a novel two-step cost function is proposed to achieve robust and efficient estimation. In contrast to the state-of-the-art method, the method proposed does not need multiple overlapped antennas and can resolve multiple targets in the same range and Doppler bins. The proposed method has been verified with numerical simulations with different parameter settings, as well as experimental data from a radar target simulator.**

***Index Terms*—Automotive radar, Doppler de-aliasing, multiple-input–multiple-output (MIMO) array, time-division-multiplex mode (TDM).**

NOMENCLATURE

α_i	Constant complex amplitude related to the characteristics of the target i.
B	Bandwidth of the RF signal.
c	Speed of light.
D_i	Round-trip distance between the ith target and the transmitter and receiver antennas at time t.
f_0	Starting frequency of the RF signal.
f_s	Sampling frequency in the fast time.
f_v	Frequency in the slow time.
$f_{d,i}$	Doppler frequency of the ith target.
K_d	Total number of samples in one chirp.
k	Fast time index.
L_d	Total number of chirps in one frame.
l	Slow time index.
M_r	Number of receive antennas.
M_t	Number of transmit antennas.
p	Index of the transmit antenna.
q	Index of the receive antenna.
r_i	Received signal of the ith target.
$s(t)$	Signal model FMCW.
s_{settle}	Settling time.
t	Variable for time.
t'	Variable of the fast time.
T	Pulse repetition time (PRT).
T_c	Chirp duration.
τ_i	Round-trip delay of the reflected signal for the ith target.
θ	Azimuth angle.
v_r	Doppler velocity, that is, the relative radial velocity between the radar and the target measured with the Doppler effect.
V_{ma}	Maximum unambiguous Doppler velocity.
$z_i(l, t')$	De-chirped received signal for the ith target.
μ	Frequency modulation rate.

Received 22 May 2025; revised 11 September 2025; accepted 4 October 2025. Date of publication 20 October 2025; date of current version 7 November 2025. This work was supported by the Dutch Research Council NWO under M2 Grant "NERD". The Associate Editor coordinating the review process was Dr. Gang Yu. *(Corresponding author: Tworit Dash.)*

The authors are with the Microwave Sensing, Signals and Systems (MS3) Group, Delft University of Technology, 2628 CD Delft, The Netherlands (e-mail: s.yuan-3@tudelft.nl; t.k.dash@tudelft.nl; i.roldanmontero@tudelft.nl; f.fioranelli@tudelft.nl; a.yarovoy@tudelft.nl).

Digital Object Identifier 10.1109/TIM.2025.3623765

I. INTRODUCTION

AUTOMOTIVE radar can provide accurate and direct measurements of the range, relative radial velocity, and angle of multiple targets, as well as a long-range coverage of over 200 m, even in challenging weather or lighting conditions [1] outperforming other sensors, namely camera and Lidar. As per relevant requirements, radar has changed its role from a detection sensor to an imaging sensor, providing a robust and reliable spatial sensing ability. The imaging quality relies on the radar's resolutions in space and angles.

Frequency-modulated continuous-wave (FMCW) radar is known for its simultaneous range and Doppler velocities estimation, relatively low sampling frequency with de-chirping technique, safety with low transmitted power, low cost, portable size, and high reliability, making it one of the most widely used radars in many applications [2]. Angular resolution is contingent upon the antenna aperture and thus is determined by the number and placement of the transmit and receive antenna elements, limited by the radar cost and packaging size. Multiple-input–multiple-output (MIMO) radar technology [3] exploits the spatial diversity of transmit and receive antenna arrays and can provide direction-of-arrival (DOA) estimation at the same accuracy level with a relatively lower number of antennas, making it competitive for many applications in automotive and beyond, that is, imaging [4], [5], gesture and pose recognition [6], [7], and heartbeat sensing [8]. To realize MIMO operational mode, signals transmitted from different transmitters have to be orthogonal to each other.

Frequency (Doppler)-division multiplexing techniques for MIMO are widely used in the current generation of automotive MIMO radars. However, this technique decreases the unambiguous Doppler interval of the radar proportionally to the number of transmit antennas. Code-division multiplexing technique uses a variety of mutually orthogonal waveforms for transmit antennas. Different code families, namely random, Gold [9], zero correlation zone (ZCZ) [10], and Kasami codes [11], are optimized for periodic autocorrelation properties. However, they still exhibit reasonable aperiodic autocorrelation properties, which means that the required orthogonality cannot be achieved perfectly. This will increase the sidelobe levels and worsen the beam pattern for the MIMO radar system, by extension, degrading the performance of DOA estimation. The time-division-multiplex access mode can avoid the disadvantages of the frequency-division method. Also, due to the simplicity and practicability of the time-division-multiplex mode (TDM), it is the primary option for co-located MIMO radars [12].

Although the TDM of transmit elements offers an orthogonality approach with low hardware complexity, it is susceptible to phase errors in nonstationary scenarios. Various TDM transmission schemes exist. For example, in one approach, each transmitter sequentially transmits the entire chirp sequence while the RF remains active. However, this can lead to azimuthal target motion between measurements from different transmitters, severely. To mitigate this, an alternative scheme allows each transmitter to send only one chirp per cycle, repeating across the frame, thereby reducing the impact of azimuthal movement. Several studies have addressed this limitation of TDM MIMO systems. A random antenna activation pattern is proposed in [13] to solve the limitations of the TDM for platform movement, by a stationary target shift in the reconstructed image. The DOA estimation errors caused by the motion-induced phase for TDM are compensated in [14].

Since each transmitter of the TDM MIMO transmits a signal at a different time, the equivalent PRF in TDM MIMO schemes equals the PRF of the other MIMO schemes divided by the number of transmit channels. Consequently, the PRT increases, leading to the shrinking of the unambiguous Doppler velocity range for Doppler processing. As a result, fast-moving targets and even the environmental clutter have velocities above the unambiguous Doppler threshold and consequently appear in wrong Doppler/velocities bins (so-called Doppler aliasing [15]) in the range–Doppler plane and mask reflections of weak targets. To overcome this effect, either the PRF of transmitted signals should be made very high, which reduces the unambiguous range of the radar (the range–Doppler dilemma), or dedicated processing methods to resolve Doppler ambiguity need to be implemented. For a cascaded radar board with a large number of transmitters offering better spatial sensing ability, this issue is severe [16]. De-aliasing the Doppler velocity in the TDM MIMO radar board is thus very important for radar applications. The problem of shrinking the unambiguous Doppler/velocity range in Doppler estimation is addressed in [17] and [18] by comparing the phase offsets in the virtual antenna. Those phase comparison algorithms are easily affected by the phase noise. The method in [17] requires the target angle information to be known a priori, and [18] needs multiple overlapped antennas with different activation time differences. However, all the aforementioned methods assume that each range-Doppler bin contains only one target, making it less practical for real applications.

In this article, a novel Doppler de-aliasing approach has been proposed to resolve Doppler ambiguity in TDM MIMO by activating one transmitter twice and implementing a two-step cross-entropy-based method. The state-of-the-art method requires each range–Doppler bin to contain only one target, while our method requires only one target per range–angle bin. The proposed method can successfully handle scenarios where multiple targets lie within the same range–Doppler bin, but they are located at different spatial positions, a case in which the state-of-the-art method fails.The repeated transmitter forms an overlapped array to spatially resolve the targets. Then, the closed form of the Doppler ambiguity signal about TDM MIMO is derived, and the Doppler de-aliasing algorithm is proposed using two-step cross-entropy optimization. The proposed method has been verified with numerical simulation results and experimental data from the radar targets simulator, demonstrating good results.

The remainder of this article is organized as follows. In Section II, the MIMO array and the signal model for the TDM Doppler signal are provided. The problem formulation and the proposed method are demonstrated in Section III. The results for simulated targets and experimental data are provided in Section IV. Finally, Section V concludes the article.

II. Signal Model

An FMCW MIMO radar with $M_{\mathbf{t}}$ transmit and $M_{\mathbf{r}}$ receive antennas is considered here. The antenna array is assumed linear, where $\mathbf{x}_{\mathrm{TX}}$ and $\mathbf{x}_{\mathrm{RX}}$ are the positions of the transmitter and receiver, respectively. The index of the transmit antenna elements is denoted by $p \in [0,\ M_{\mathbf{t}} - 1]$ sorted by order of activating time according to the TDM scheme, and the index of the receive antenna elements is denoted by $q \in [0, M_{\mathbf{r}} - 1]$.

The FMCW chirp is transmitted with duration T_c, bandwidth B, and pulse repetition interval (PRI) T and has the form

$$s_0(t) = \begin{cases} e^{j2\pi\left(f_0 t + 0.5\mu t^2\right)}, & t \in [0, T_c] \\ s_{\mathrm{settle}}(t), & t \in [T_c, T] \end{cases} \tag{1}$$

where f_0 denotes the starting frequency, $\mu = (B/T_c)$ denotes the frequency modulation rate, and $s_{\mathrm{settle}}(t)$ indicates the signal during the settling time of the radar.

The periodic transmitted signal with the continuous time flow t is decomposed into fast-time domain t' and chirp number domain $l = \lfloor (t/T) \rfloor$ with $t' = t - lT$, $t' \in [0, T_c]$. The notation $\lfloor x \rfloor$ indicates the floor function (i.e., it indicates the greatest integer less than or equal to x), hence $l = 0, 1, 2, \ldots, L_d - 1$, where L_d is the total number of chirps in one frame. A visual illustration is shown in Fig. 1, where t refers to the continuous time flow, t' is the variable of the fast time, and l represents slow-time indexes for later processing.

Thus, the periodic sequence of chirps can be expressed as

$$s(t) = s\left(t' + \mathrm{lT}\right) = s\left(l, t'\right) = s_0\left(t'\right). \tag{2}$$

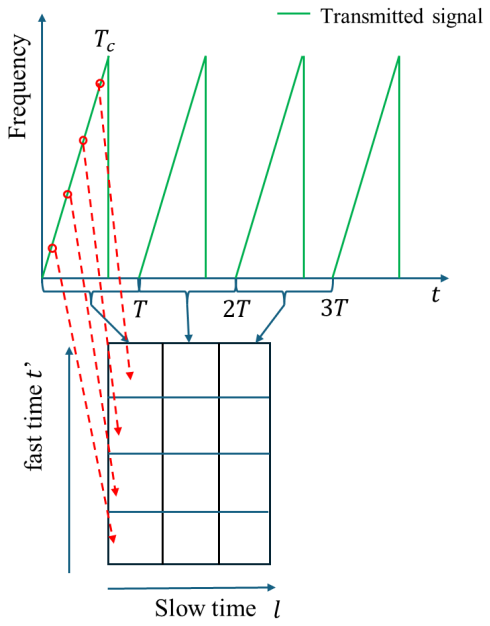

Fig. 1. Illustration of the FMCW signal model.

In the absence of multiscattering effects over the targets, the multitarget signal is the summation of several single-point targets' signals. To illustrate the signal model, the radar signal is derived first based on a single-point target signal and extended to a multitarget signal at the end. The round-trip delay of the reflected signal for the i target is

$$\tau_i\left(l,t'\right) = \frac{2\left(D_i\left(t'+\mathrm{lT}\right)+v_r\left(t'+\mathrm{lT}\right)\right)}{c} \approx \gamma_i + \frac{2v_r\left(t'+\mathrm{lT}\right)}{c} \tag{3}$$

where c is the speed of light, $D_i(t)$ is the round trip distance between the ith target and the transmitter and receiver antennas at time t, v_r is the radial velocity between the radar and the target, and $\gamma_i = (2D_i(t'+\mathrm{lT})/c) \ll T_c$. The corresponding received signal can be written as

$$r_i\left(l,t'\right) = \alpha_i s\left(t'+\mathrm{lT}-\tau_i\left(l,t'\right)\right) \quad \text{with } t' \in \left[\gamma_i, T_c\right] \tag{4}$$

where α_i is the constant complex amplitude related to the characteristics of target i.

The received signal is then correlated with the complex conjugate of the transmitted signal $s^*(l,t')$ to obtain the de-chirped signal z_i as

$$z_i\left(l,t'\right) = r_i\left(l,t'\right) \times s^*\left(l,t'\right). \tag{5}$$

This de-chirped signal will be sampled with respect to fast time with frequency f_s, and the discretized signal $\hat{z}_i$ in the time domain, considering the geometry of MIMO, is obtained as

$$z_i^{(d)}(l,k) \approx \alpha_i \exp\left[j2\pi\frac{f_0}{c}\left[\mathbf{x}_{\mathrm{TX}}(p)+\mathbf{x}_{\mathrm{RX}}(q)\right]\sin\theta_i\right] \times \exp\left[j2\pi\left(f_{d,i}\mathrm{Tl}+\mu\frac{D_i(l)}{c}\frac{k}{f_s}\right)\right] \tag{6}$$

where the superscript (d) represents the discretized version, $k = 0,1,2,\ldots,K_d-1$, where $K_d = T_c f_s$ is the maximum number of samples within one chirp, $f_{d,i} = (2v_{ri}f_0/c)$ is the Doppler frequency of the target i, v_{ri} is the radial velocity of the target i, and θ_i is the azimuth angle of the targets.

The orthogonality of the transmitter is achieved by activating different transmitters at different slow times, the so-called TDM, meaning that p in (6) is linked to the slow time l.

In the conventional case without TDMA, the chirp index l directly corresponds to the slow-time index, that is,

$$l = \text{slow-time index}, l = 0,1,\ldots,L_d.$$

However, in a TDMA configuration with M_t transmit antennas, this one-to-one correspondence no longer holds. Each chirp index l now can be uniquely decomposed into a pair (n,p), where n is the new slow-time index, as follows:

$$l = (n-1)M_t + p. \tag{7}$$

Equivalently, the mapping between the conventional chirp index l and the pair (n,p) is given by

$$n = \left\lfloor \frac{l}{M_t} \right\rfloor, \quad p = (l) \bmod M_t. \tag{8}$$

Thus, in TDMA systems, the chirp index l must be redefined into two indices.

1) n: the new slow-time index, used for Doppler processing.
2) p: the transmit antenna index.

Because of this coupling between Doppler and angle information, the signal becomes

$$z_i^{(d)}(p,q,l,k) = \sum_{i=1}^{k_s}\alpha_i \exp\left[j2\pi\frac{f_0}{c}\left[\mathbf{x}_{\mathrm{TX}}(p)+\mathbf{x}_{\mathrm{RX}}(q)\right]\sin\theta_o\right] \times \exp\left[j2\pi\left(f_{d,i}M_tT\left\lfloor\frac{l}{M_t}\right\rfloor + f_{d,i}\mathrm{pT}\right)\right] \times \exp\left[\mu\frac{D_i(n)}{c}\frac{k}{f_s}\right)\Bigg]. \tag{9}$$

For the MIMO radar with $M_{\mathbf{t}}$ transmit and $M_{\mathbf{r}}$ receive antennas, if all positions of TX and RX antenna elements were separated, one obtains $M_{\mathbf{t}} \times M_{\mathbf{r}}$ received signals in total. In this case, an MIMO setup can be equivalently substituted by a single transmit antenna at position 0 and by $M_{\mathbf{t}} \times M_{\mathbf{r}}$ receive antennas. This equivalent single-input–multiple-output antenna array setup is called the virtual array. The virtual array analysis is important for MIMO techniques, as it links MIMO arrays and the classical array synthesis technique. The presence of "overlapped antenna elements" means having specific transmitters and receivers in the same position D in the virtual array analysis

$$D = \mathbf{x}_{\mathrm{TX}}(p) + \mathbf{x}_{\mathrm{RX}}(q) \quad \forall (p,q). \tag{10}$$

When the number of scatter points in the field of view is equal to k_s, the total signal is constructed by superposition

$$z^{(d)}(p,q,l,k) = \sum_{i=1}^{k_s}\hat{z}_i^{(d)}(p,q,l,k). \tag{11}$$

III. Problem Formulation and Discussion

A. Problem Formulation

The number of transmitters working in the TDM mode will significantly reduce the measurable, unambiguous target velocity, limiting the radar's velocity-sensing ability. Conventional Doppler processing uses only the signal from one fixed transmitter. In this case, the phase difference of a single target is $\Delta\phi = 2\pi f_0((2v_i/c)M_tT)$. The phase difference should be $|\Delta\phi| < \pi$ to avoid ambiguity. Hence, one can obtain the maximum unambiguous Doppler velocity as $V_{\text{ma}} = (c/4TM_tf_0)$. The maximum unambiguous Doppler velocity is thus negatively correlated to the number of transmitters.

Moreover, all transmitted signals contain the full Doppler information with maximum unambiguous Doppler: $V_{\text{ma}} = (c/4Tf_0)$. However, the Doppler information is coupled with the transmitter activating time, as shown in (9). The Doppler phase difference of the single target becomes $\Delta\phi = 2\pi f_0(\,(2v_i/c)M_tT\lfloor(l/M_t)\rfloor + (2v_i/c)\text{pT})$. Thus, directly using all the chirp information in TDM mode makes it impossible to extract the right Doppler information.

A robust, reliable, and accurate Doppler velocity estimation is needed for MIMO arrays in the TDM mode, especially if the application requires high spatial resolution, like the cascade radar boards with more transmitters used in automotive.

B. Analysis of the Signal

The aforementioned problem is complicated because one notices that the array signal is fully coupled with the slow-time sampled signal. Observing the signal in (9), the problem can be simplified in the first stage by designing an overlapped antenna according to Section II to make the first term $(e^{j2\pi(f_c/c)[\mathbf{x}_{\text{TX}}(p)+\mathbf{x}_{\text{RX}}(q)]\sin\theta_i})$ constant. Then, the problem can be simplified into how to retrieve Doppler velocity information from the resulting raw signal in (12). For simplification without losing generality, the index k_s is set to 1 for discussion, which can be obtained by implementing an FFT along the range and the antenna array, so that one bin contains information of one target

$$z^{(d)}(p,l) = \sum_{i=1}^{k_s} \alpha_i e^{j2\pi f_0\left(\frac{2v_i}{c}M_tT\lfloor\frac{l}{M_t}\rfloor + \frac{2v_i}{c}\text{pT}\right)} \tag{12}$$

where $\alpha_i = a_i e^{j2\pi(f_c/c)[\mathbf{x}_{\text{TX}}(p)+\mathbf{x}_{\text{RX}}(q)]\sin\theta_i}$ by merging the array signal with the targets' reflectivity.

1) Here, if $p = 0$, this means that the TDM is not implemented at all. Then, the signal can be processed by the conventional Doppler DFT to estimate the DFT value at frequency f_v as

$$F(f_v) = \text{sinc}\left(\frac{L_d\left(f_v + f_{d,i}\right)}{2}\right). \tag{13}$$

2) If $p = \vec{p}_o = 0 : N_t - 1$, this means that the transmitters of those overlapped antennas are activated one by one, and the schematic of this signal in the example case of $N_t = 4$ is shown in Fig. 2. Then, the absolute value of the signal in (12) after DFT at frequency f_v is equal to

$$F(f_v) = \text{sinc}\left(\frac{N_t\left(f_v + f_{d,i}\right)}{2}\right) \times \text{sinc}\left(\frac{(L_d \times M_t)\left(f_v + f_{d,i}\right)}{2}\right). \tag{14}$$

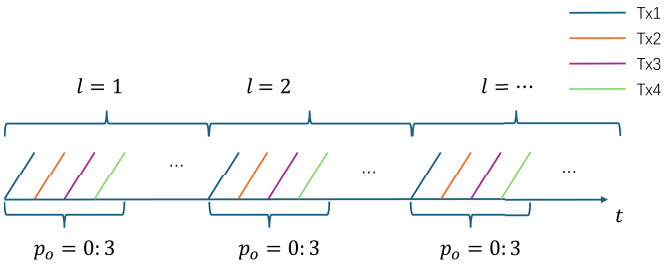

Fig. 2. Example of a schematic of the Doppler signals for the overlapped antennas. In this case, the number of overlapped antennas is equal to 4. The four different colored lines represent the signal from the overlapped antenna in space formed by different transmitters. The other transmitters will still be active, but without contributing to this overlapped antenna position, which is represented by three dots in between the highlighted colored lines in the figure.

3) If $p \overset{i.i.d.}{\sim} \mathcal{U}[1,\ N_t]$, this means that the transmitter to form the overlapped antennas is activated randomly, and the DFT of such a signal becomes equal to the closed form of nonuniform DFT. This signal will have no closed form, and Doppler information cannot be de-aliased with the proposed frequency-model-based method.

C. Proposed Method

The analysis from Section III-B shows that if the MIMO array working in TDM mode can be designed to form an overlapped antenna and those formed overlapped antennas are transmitted in sequential order, then the frequency function of the signal will have a closed-form mathematical formula. This can be achieved by activating one transmitter twice, meaning changing from the conventional activating order of TDM "tx1–tx2–tx3" to "tx1–tx2–tx2–tx3…." By doing repetitive transmission from the same transmitter, the period between two sequential measurements of Doppler is decreased, and consequently, this gives an opportunity to increase the unambiguous velocity. The whole method can be seen as aperiodic measurements of Doppler: TX1—large PRI, TX2—small PRI, TX3—large PRI. Such a setting will not influence the range and angular processing, thus maintaining the same resolutions and maximum unambiguous range. In this case, the signal of the repeated transmitted signal, tx2 specifically, will follow the analyzed signal model (14). The Doppler unambiguous range will shrink further, but the problem will be solved in the proposed parametric approach. To achieve the Doppler de-aliasing, the block diagram of the proposed algorithm integrated into the rest of the radar processing is shown in Fig. 3.

The proposed formulation is derived based on the assumption that each Doppler cell only contains one target informa-

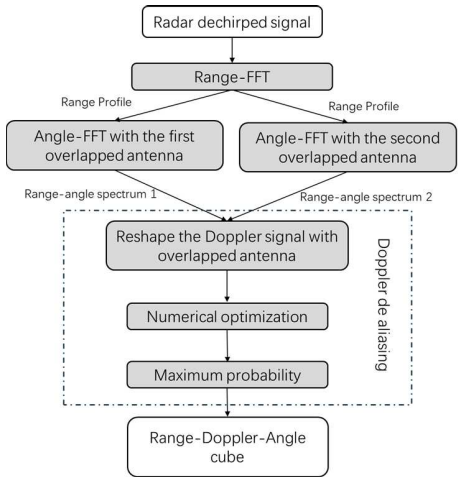

Fig. 3. Block diagram of the proposed Doppler de-aliasing integrated into the rest of the radar processing.

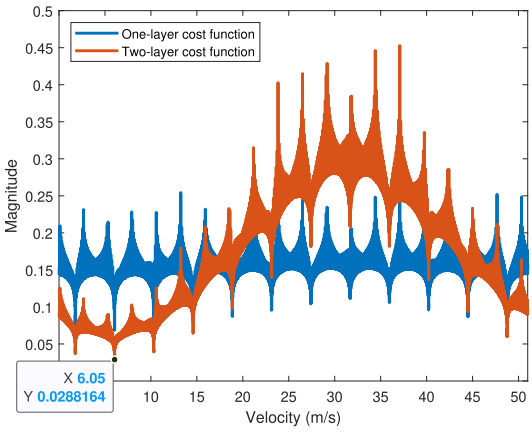

Fig. 4. Optimization function of the cross-entropy between the measurement and the model, where the blue line is the one-step optimization, and the red line is the proposed two-step optimization.

tion, which is the same assumption for all the state-of-the-art algorithms [17], [18]. To make the assumption reasonable in a dynamic target scenario, current research that only considers resolving targets in the range dimension is not enough. Thus, the overlapped antenna arrays can be formed by activating the same transmitter sequentially, and the targets can be resolved in different spatial positions first. The received radar-de-chirped signal is processed with range–FFT and angle–FFT with both overlapped antenna arrays. Then, each signal of the range–angle cell is sent to the proposed Doppler de-aliasing method. The final range–unambiguous Doppler–angle cube can be obtained.

The measured signals of the overlapped antennas in one range–angle cell are concatenated into one Doppler signal vector, sorted with the chirp indices and the activated transmitter time. The formed vector is denoted by $\mathbf{S} \in \mathbb{C}^{1\times(L_d M_t)}$ and can be reshaped from the matrix in (12) as follows:

$$\mathbf{S} = \underbrace{\left[z^{(d)}\left(\vec{p}_o, 0\right); \ldots z^{(d)}\left(\vec{p}_o, l\right), \ldots, z^{(d)}\left(\vec{p}_o, L_d - 1\right)\right]}_{(L_d M_t)}. \quad (15)$$

The DFT function of the formed vector $\mathbf{S}$ is computed as

$$\mathbf{X} = \mathbf{F}\mathbf{S} + N_p \quad (16)$$

where $\mathbf{F}$ is the DFT matrix and $N_p \in \mathbb{C}^{1\times(L_d M_t)}$ is the noise matrix.

The closed form of each signal of the range–angle cell after range and angle DFT has been given in Section III-B. The signal model $\mathbf{Y} \in \mathbb{C}^{1\times(L_d M_t)}$ is the corresponding theoretically derived function

$$\mathbf{Y}(v) = \operatorname{sinc}\left(\frac{N_t\left(i + \frac{4\pi f_0 v T_d}{c}\right)}{2}\right) \times \operatorname{sinc}\left(\frac{L_d \times M_t\left(i + \frac{4\pi f_0 v T_d}{c}\right)}{2}\right). \quad (17)$$

A theoretically derived semi-analytical definition of a Doppler periodogram for extended targets with one burst (no sample gaps) can be found in [19]. The optimization goal is to find the parameter $\hat{v}$ to achieve the similarity between the measured signal and the theoretically derived signal. The common functions to describe similarity between two vectors consist of Euclidean distance, cross-entropy, and cosine similarity. Among them, cross-entropy is more robust in the presence of noise scenarios and is thus selected as the optimization function for this work.

The problem then becomes an optimization problem, with the objective defined as $\hat{v} = \arg\min_v f_1(v)$, where $f_1(v) = -\sum_i^{L_d\times M_t} \mathbf{Y}(i)\log[\mathbf{X}(i)]$.

One example of the cost function of different values of the variable v = 6 m/s is shown with the blue line in Fig. 4. Because the periodic time gap in the formed Doppler signal is usually larger than the useful signal, this introduces a lot of harmonic peaks. The global minimum of cross-entropy is at 6 m/s. Still, this is not obvious due to the other local minima, causing the optimization process to get easily stuck in the wrong value.

Thus, a second vector is extracted from the signal in (12) as $\mathbf{S}_s = z(p, 1)$, while the DFT function $\mathbf{X}_s = \mathbf{F}\mathbf{S} + N_s \in \mathbb{C}^{1\times L_d}$ has the theoretical formula as $\mathbf{Y}_s(v) = \operatorname{sinc}((N_t(i + (4\pi f_0 v T_d/c))/2))$.

The two-step cross-entropy is proposed to deal with this challenge and is introduced as follows:

$$\hat{v} = \arg\min_v f(v) \quad (18)$$

where $f(v) = \sum_i^{L_d\times M_t} \mathbf{Y}(i)\log[\mathbf{X}(i)] \times \sum_i^{L_d\times M_t} \mathbf{Y}_s(i)\log[\mathbf{X}_s(i)]$. The new cost function is shown with the red line in Fig. 4, and the global minimum is easier to reach to provide the correct estimation. Those local minima are due to the periodical gap due to the TDM, the second sinc as shown in (17).

Different optimization algorithms can be used here, for example, the genetic algorithm [20], simulated annealing [21], and pattern search [22]. The gradient-based and pattern search methods are compared in this study to solve this optimization problem. In this way, one can obtain the estimated unambiguous Doppler velocity of the target $\hat{v}$. As shown in Fig. 4, there are many local minima; thus, the optimization is

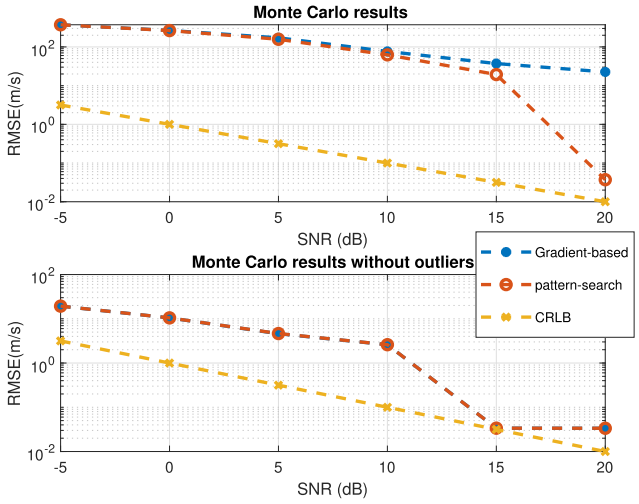

Fig. 5. RMSE from 1000 Monte Carlo tests and CRLB for the Doppler velocity estimation of algorithms, computed in different SNR conditions. The top figure shows the results without removing outliers, and the bottom figure shows the results after removing outliers, representing an infinite number of iterations.

performed at random starting points multiple times to achieve robust results.

IV. Results and Discussion

In this section, the effectiveness of the proposed method is demonstrated through the utilization of simulated ideal point targets, simulated extended targets, and experimental data.

A. Simulated Results

The MIMO TDM-FMCW radar's Doppler signal is simulated using the following parameters to evaluate the proposed method. A typical radar setting is specified as follows: the starting frequency of the FMCW chirp f_0 is 77 GHz, 128 chirps are processed in each frame, and 12 transmitters are used here for mimicking the cascaded board AWR224 by Texas Instruments (TI) [23]. The chirp duration is 25.8 us. Such a TDM radar system provides [−3.15, \; 3.15 m/s] unambiguous Doppler velocity estimation, which is insufficient for automotive applications.

Fig. 5 compares the root-mean-squared errors (RMSE) of the proposed method with the Cramér–Rao lower bound (CRLB) [24]. The target speed is randomly selected from the range [−37.8, +37.8 m/s]. Since conventional Doppler DFT cannot resolve ambiguous speeds, it is not included in the comparison. The proposed method is evaluated using both a gradient-based optimization solver and a pattern search optimization solver. As shown in Fig. 5, the RMSE decreases as the SNR increases, and as the SNR reaches 15 dB approaches the CRLB limit. The top subfigure presents results without outlier removal, where outliers essentially are the cases in which the optimizations fail to reach the global minimum because of the limited repetitions.

In this case, RMSE remains rather high in most cases due to the limited number of optimization repetitions, that is, 256 repetitions, with different starting points in both methods, which, for computational feasibility, cannot be made arbitrarily large. In an ideal scenario with infinite repetitions, the results would be equivalent to those obtained after outlier removal, as shown in the bottom subfigure. Here, both gradient-based and pattern search methods achieve similar accuracy, as expected. Notably, in the top subfigure, the pattern search method outperforms the gradient-based approach at higher SNR values, indicating that pattern search is more effective when the number of optimization repetitions is limited. This advantage arises because pattern search contains multiple optional search [22], whereas the gradient-based method follows a single search path determined by the initial optimization value.

The main advantage of using a gradient-based approach instead of pattern search is computational efficiency. Moreover, the optimization is performed multiple times with different starting points to calculate the minimal-cost positions, thereby reducing the requirement for the optimization algorithm to reach the global optimum.

The computational complexity is analyzed here before the test of different parameters. The computation of the proposed method is mainly contributed to by the FFT and the optimizations. The computational complexity of the FFT, determined by the size of FFT $L_d * M_t$, is $O(2L_dM_t\log(L_dM_t)$. The optimization is determined by the iteration of the optimization $N_r * N_b$, where N_r is the number of optimization iterations performed at random starting points and N_b is the number of iterations needed for each optimization to reach the minimum and the cross-entropy operations. The computational complexity of each cross-entropy is $O(L_dM_t)$, so the total cost of the optimization is $O(N_rN_bL_dM_t)$. The computation complexity of the proposed method is $O(L_dM_t(\log(L_dM_t)+(N_rN_b)$. It is worth mentioning that the optimization can be computed in parallel, thus reducing the time consumption.

To compare computational efficiency, 500 Monte Carlo tests were performed using different optimization methods on a computer with an Intel Xeon Platinum 8358P CPU, without parallel computing. On average, the pattern search method required 8.173 s, whereas the gradient-based method required only 3.924 s, demonstrating that the gradient-based approach is more than twice as fast as pattern search.

To validate the effectiveness of the proposed two-layer cost function, 500 Monte Carlo tests with different optimization models were conducted. The time required for the one-layer cost function is 1.969 s, while the proposed two-layer cost function requires only 3.924 s. However, the estimation accuracy decreases significantly with respect to the two-layer approach, specifically 0.03 versus 2.80 m/s, highlighting the accuracy improvement achieved by the proposed two-layer model despite the heavier computational cost. It should be noted that the reported time does not include parallel computing; the method could be further accelerated using advanced processing units, which is beyond the scope of this work.

Additionally, different parameters are tested to show their influence on the estimation performance, that is, the number of chirps used in total, and the number of MIMO transmitters.

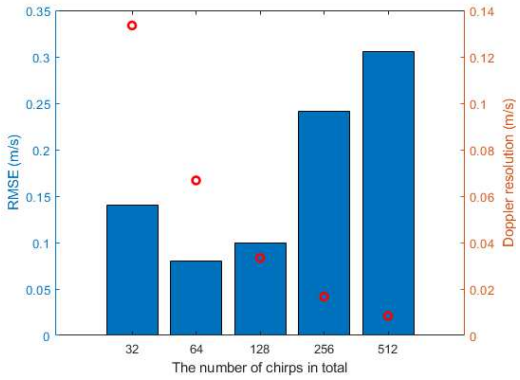

Fig. 6. RMSE of estimated error in 1000 Monte Carlo tests with different numbers of chirps used. The left blue axis is the estimated RMSE and the right red axis is the Doppler resolution of each setting.

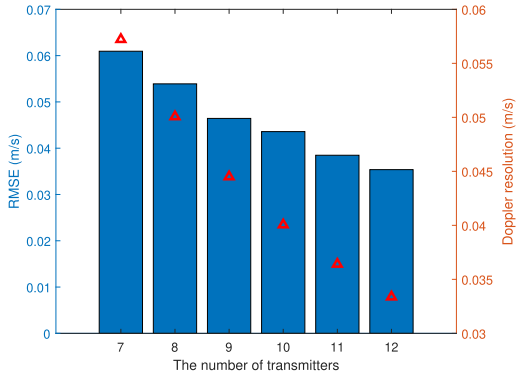

Fig. 7. RMSE of the estimated error in 1000 Monte Carlo tests with different numbers of transmitters used.

The results in terms of estimated error with different numbers of chirps for Doppler velocity estimation are shown in Fig. 6. The simulation is performed with 12 transmitters operating in the TDM mode, with results averaged over 1000 Monte Carlo tests, where Doppler velocity is changed between [−25.6,25.6 m/s]. As expected, increasing the number of chirps improves Doppler resolution, as indicated by the red circles. Initially, the overall estimation error decreases as more chirps accumulate, providing additional target information and enhancing accuracy. However, beyond a certain point, 128 chirps in our limited simulations, the error begins to increase. This occurs because the introduction of more chirps leads to more gaps during the formation of the signal (15), and additional harmonic frequency components appear after FFT, making the optimization process more prone to converge to a local minimum rather than the global optimum. These results highlight a tradeoff between Doppler resolution and estimation accuracy in this context.

The results illustrating the relationship between the total number of transmitters and the estimated errors in velocity are shown in Fig. 7. One of the antennas is activated twice sequentially as proposed. The number of chirps used for Doppler processing remains constant at 128, meaning that the total observation time increases with the number

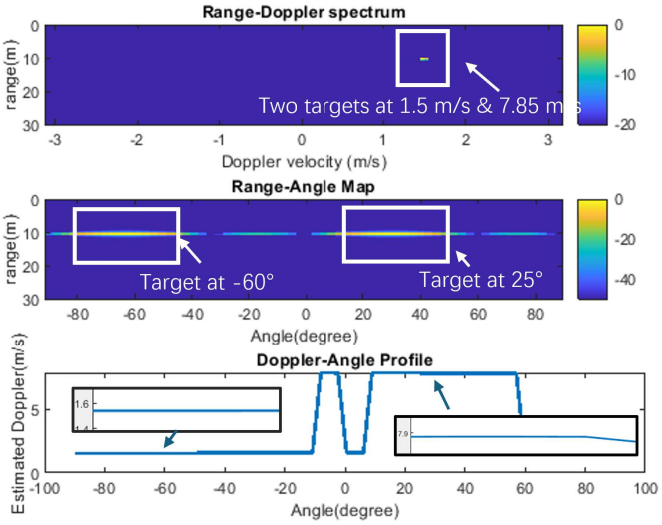

Fig. 8. Top figure is the range–Doppler spectrum of two targets, where one moves at 1.5 m/s (within the unambiguous Doppler velocity range) and another at 7.85 m/s (outside the unambiguous Doppler velocity range). The middle figure is the range–angle map of these two targets. The bottom figure is the estimated Doppler velocity profile generated by our proposed estimation method.

of transmitters. This increase in observation time improves Doppler resolution. As a result, a decrease in estimated error is observed as the number of transmitters increases, due to enhanced Doppler resolution. More transmitters lead to a smaller unambiguous Doppler range, which can be mitigated using the proposed method. However, longer observation periods also result in higher latency and increase the risk of target migration problems. For the number of transmitters M_t, the latency for a frame is equal to $T_{\text{CPI}} = N * T_{\text{prt}}$. So, the latency will be proportional to the number of transmitters. The range migration across the CPI $M_R = (|v_r|T_{\text{CPI}}/c/2B)$ is also proportional to the number of transmitters, indicating that if more antennas are used, a higher migration risk will happen. When M_R is smaller than 0.5, usually the migration effect is acceptable. Therefore, despite the improved accuracy with more transmitters, the number of transmitters cannot be set too high.

To test the proposed method's performance on multiple target cases, ideal point targets and extended targets are simulated in the following tests. The two ideal point targets are placed in the same range bin. The results of two ideal point targets are shown in Fig. 8. The Doppler spectrum is aliased in the unambiguous range, so the two targets at 1.5 and 7.85 m/s in the simulation are merged into one same range–Doppler bin, as shown in the top subfigure. Using the proposed overlapped antenna array, the two targets are separated in the azimuth dimension as shown in the middle subfigure. Then, the Doppler de-aliasing method is implemented on the two targets, respectively. The results for both targets are correctly estimated as moving at 1.51 m/s for the target at −60° and 7.3 m/s for the target at 25°. The profile highlights the estimated velocity for those range–angle bins where targets exist. The detection process can discard the areas where no targets are present.

Additionally, the method in [18] is implemented on the same scenario. Since the two targets' information is merged

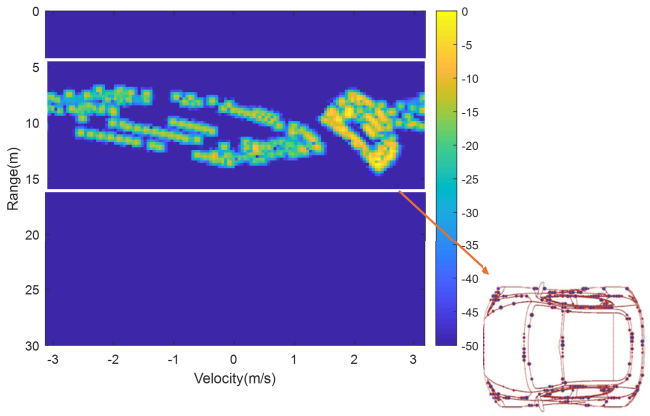

Fig. 9. Range–Doppler spectrum of two cars. The used extended car model with 273 point scatterers is shown at the bottom-right of the figure. One car model is moving at 3 m/s (within the unambiguous Doppler velocity range), and another at 15.6 m/s (outside the unambiguous Doppler velocity range). The spreading of the Doppler signature is because the car is spatially extended in different azimuth angles.

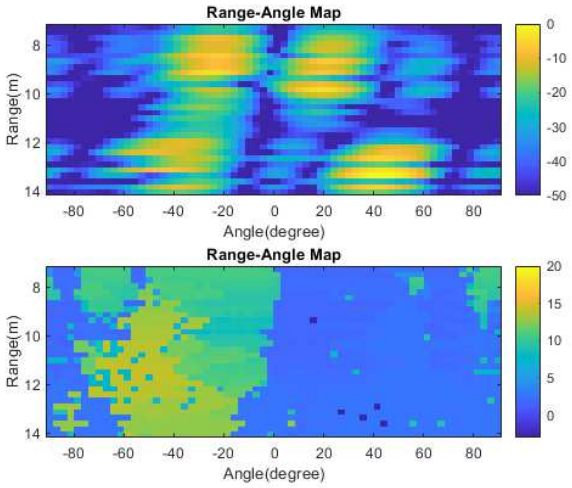

Fig. 10. Range–angle maps of two simulated car models, where the left one with respect to zero degrees angle is moving at 15.6 m/s and the right one is moving at 3 m/s. Top figure: the color is mapped by the received intensity. Bottom figure: the color is mapped by the estimated Doppler velocity.

into the same range–Doppler bin, the method [18] provides an estimate at 4.8843 m/s, which corresponds to the theoretical center position (4.675 m/s) between the two targets' Doppler velocities (7.85 and 1.5 m/s). This proves that when multiple targets are merged into the same range–Doppler bin, the state-of-the-art method [18] fails, while our proposed method still provides reliable estimations.

Simulated models of vehicles perceived as extended targets are used for verification as well. Each car model is represented by 273-point scatterers generated randomly from the edges of the car, as shown at the bottom right in Fig. 9. The range–Doppler spectrum is shown at the top left. The Doppler spectrum is spreading because the car model represents an extended target, so that every part of the car will have different Doppler speeds. Two car models moving at 3 m/s and 15.6 m/s are simulated here, and they partially overlap with each other

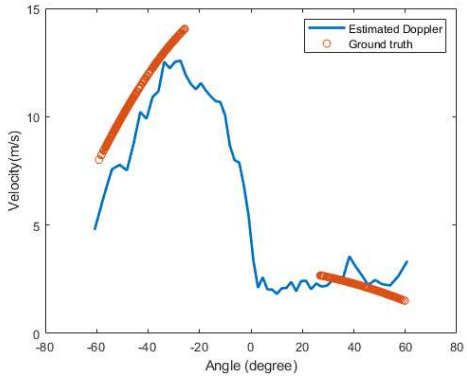

Fig. 11. Plot of estimated mean Doppler velocity and the ground-truth velocity with the azimuth angles.

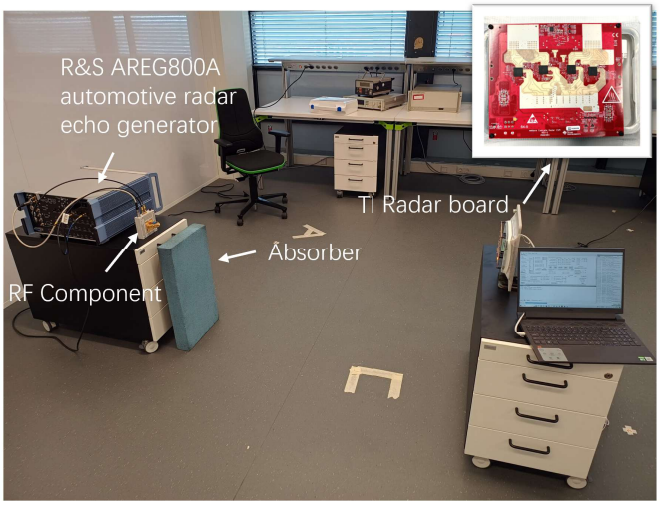

Fig. 12. Experimental setup, where the left side shows the radar target simulator, and the right side shows the TI cascaded radar board.

in the same range–Doppler bin in a way that is similar to the ideal point target. Using the formed overlapped antenna array, the two targets are separated in the azimuth dimension, as shown in the top subfigure in Fig. 10. Then, the Doppler de-aliasing method is implemented on the two car models. The results for both targets are estimated as shown in the bottom subfigure of Fig. 10, color-mapped by the estimated velocity, where the left area with yellow color indicates the estimated value around 10–13 m/s and the right area with blue color indicates with estimated value around 1–3 m/s. The estimated values are calculated with a mean operation for a 2-D visualization as shown in Fig. 11. The estimated value for the target exists area that matches the ground-truth curve, proving the effectiveness of the proposed method.

B. Experimental Data

The proposed approach is verified using experimental data collected with the TI MMWCAS-RF-EVM cascade radar board AWR2243 [23], shown at the top right in Fig. 12. The radar has 12 transmitters and 16 receivers with a formed MIMO array of 86 virtual antennas in azimuth and 4 antennas in elevation, and 32 overlapped antenna pairs in total. The

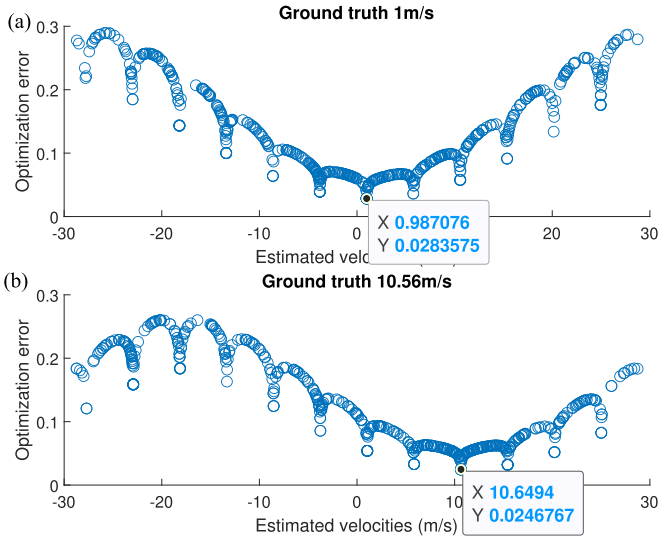

Fig. 13. Results of estimated Doppler velocity for the Radar Target Simulator, where the X value is the estimated velocity and Y value is the optimization error. In (a), the target moves at 1 m/s and in (b), the target moves at 10.56 m/s.

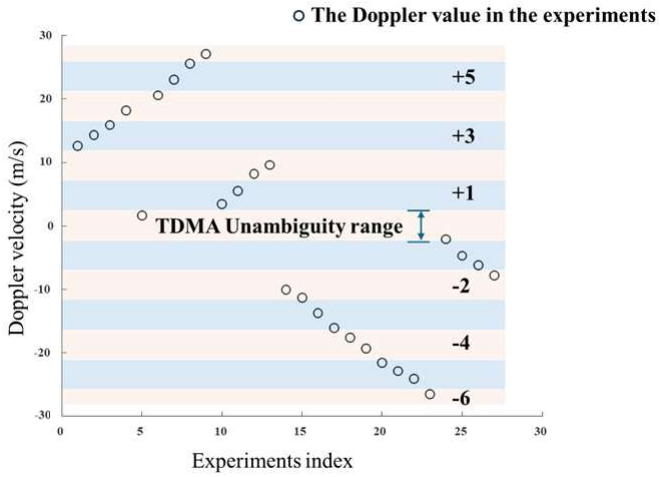

Fig. 14. Doppler velocity set for the experimental Monte Carlo tests.

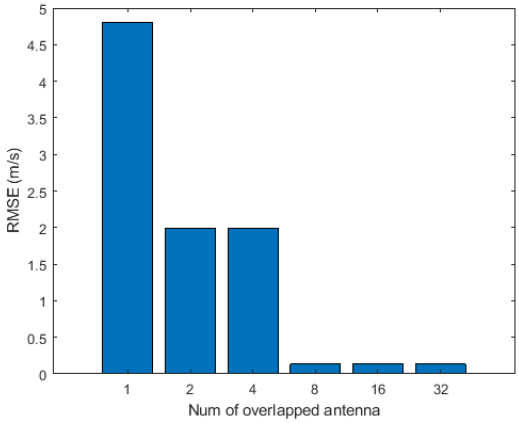

Fig. 15. Results of the state-of-the-art algorithm [18] under different numbers of overlapped antennas.

starting frequency of the generated waveform is 77 GHz, and the number of chirps is 128 for Doppler processing. The PRI is 5.5 ms. With these waveform parameters, the maximum unambiguous velocity is 4.18 m/s, and the velocity resolution is 0.033 m/s. It should be noted that these parameters are typical for automotive radar for a decent range–Doppler observation. However, the maximum unambiguous velocity is far too low for practical users due to the cascaded board containing 12 transmitters used in TDM. As shown in Fig. 12, on the left-hand side, there is an R&S AREG800A automotive radar echo generator. An RF component is then connected to the echo generator to generate the simulated target echo with the aforementioned parameter, and an absorber is placed to avoid the strong reflection from the table, while on the right-hand side, the TI radar board is located.

The echo of a target with velocity 1 m/s is emulated first. Later, the echo at the same position but with a different velocity equal to 10.56 m/s is emulated to verify that the proposed method can estimate not only the unambiguous velocity, but also the ambiguous one. The results are shown in Fig. 13. For scenario 1, where the ground-truth velocity is 1 m/s, the estimation is 0.9871 m/s. Another scenario, scenario 2, is shown in the bottom subfigure, where the ground-truth velocity is 10.56 m/s, and the estimator provides 10.64 m/s. Both results are close to the ground truth, proving the effectiveness of the proposed method.

To compare with a state-of-the-art algorithm, the algorithm proposed in [18] is chosen as the most commonly used one. This algorithm needed multiple overlapped antennas, which the TI board provided. However, compared to this algorithm, the proposed method only requires one overlapped antenna, which can maximize the angular resolution capabilities of MIMO. The algorithm in [18] estimates the velocity of scenario 1 at 0.9739 m/s, while it estimates the target in scenario 2 moving at 10.48 m/s, achieving similar results to the proposed estimator, but with stricter requirements on the number of overlapped antenna pairs, that is, using 32 in total in the TI radar board.

To investigate the method performances quantitatively, a more comprehensive comparison is conducted by redoing the Monte Carlo test for the experiment setup 540 times, namely 27 different Doppler speed values and 20 times independently collected data. The Doppler velocity for each experiment is uniformly sampled within the maximum ambiguous Doppler range, as shown in Fig. 14. The RMSE of the 540 results is calculated as 0.0448 m/s, proving the effectiveness of the proposed method, while the state-of-the-art method using 32 overlapped antennas achieves a higher RMSE of 0.1329 m/s.

Moreover, different numbers of overlapped antennas were tested using the method in [18]. The corresponding results are presented in Fig. 15. It can be observed that the estimation error decreases as more overlapped antennas are introduced, whereas the case with only one overlapped antenna produces unreliable results. Although the performance improves with a larger number of antennas, the state-of-the-art method still requires each range–Doppler bin to contain only a single target, which does not always hold in practice. In contrast, the proposed method first separates targets in the spatial domain

and assumes that each spatial position contains only one target, which is a more realistic assumption in real-world scenarios.

The edge of the unambiguous Doppler/velocity range is always challenging for conventional Doppler FFT due to the energy leakage, and so this is also the case for the proposed method. An experiment test is implemented with target velocity values of 27.1 m/s, where the maximum unambiguous velocity is 28.58 m/s, with 23 frames. The estimated results are fluctuating between the positive and negative sides, with an average of 27.0983 and −25.3266 m/s; this is a similar phenomenon to what is also occurring in the method [18].

V. Conclusion

A novel MIMO antenna array transmission mode and Doppler de-aliasing technique for TDM have been proposed to solve the Doppler ambiguity in TDM MIMO array processing. The numerical simulations and the experimental results prove the effectiveness of the proposed method. The TDM Doppler signal model has been derived, and a novel two-step cost function is proposed to achieve robust and efficient estimation. The simulation results support the idea that activating one transmitter in sequential order can effectively solve the Doppler ambiguity from the TDMA setting with the proposed method. The method achieves an error similar to that of the state-of-the-art method in the experimental data, within the error 1%, while the state-of-the-art method needs multiple overlapped antennas and cannot resolve multiple targets in the same Doppler and range cell.

References

[1] F. Engels, P. Heidenreich, A. M. Zoubir, F. K. Jondral, and M. Wintermantel, "Advances in automotive radar: A framework on computationally efficient high-resolution frequency estimation," *IEEE Signal Process. Mag.*, vol. 34, no. 2, pp. 36–46, Mar. 2017.

[2] A. G. Stove, "Linear FMCW radar techniques," *IEE Proc. F Radar Signal Process.*, vol. 139, no. 5, pp. 343–350, 1992.

[3] S. Sun, A. P. Petropulu, and H. V. Poor, "MIMO radar for advanced driver-assistance systems and autonomous driving: Advantages and challenges," *IEEE Signal Process. Mag.*, vol. 37, no. 4, pp. 98–117, Jul. 2020. [Online]. Available: https://ieeexplore.ieee.org/document/9127853/

[4] J.-H. Park, S. Lee, G. Moon, and S.-C. Kim, "Spatial-wideband effect compensation for high-resolution imaging in MIMO FMCW radar," *IEEE Trans. Instrum. Meas.*, vol. 73, pp. 1–12, 2024.

[5] S. Yuan, F. Fioranelli, and A. G. Yarovoy, "3DRUDAT: 3D robust unambiguous Doppler beam sharpening using adaptive threshold for forward-looking region," *IEEE Trans. Radar Syst.*, vol. 2, pp. 138–153, 2024.

[6] X. Wang, H. Liu, X. Wang, V. C. Chen, M. G. Amin, and K. Cai, "Sensing, tracking, and recognition of macro–micro hand gestures using interferometric MIMO radar," *IEEE Trans. Instrum. Meas.*, vol. 73, pp. 1–14, 2024.

[7] C. Wang, D. Zhu, L. Sun, C. Han, and J. Guo, "Real-time through-wall multiperson 3-D pose estimation based on MIMO radar," *IEEE Trans. Instrum. Meas.*, vol. 73, pp. 1–11, 2024.

[8] Z. Li, T. Jin, Y. Dai, and Y. Song, "Motion-robust contactless heartbeat sensing using 4-D imaging radar," *IEEE Trans. Instrum. Meas.*, vol. 72, pp. 1–10, 2023.

[9] O. S. Rothaus, "Modified gold codes," *IEEE Trans. Inf. Theory*, vol. 39, no. 2, pp. 654–656, Mar. 1993.

[10] Y.-C. Liu, C.-W. Chen, and Y. T. Su, "New constructions of zero-correlation zone sequences," *IEEE Trans. Inf. Theory*, vol. 59, no. 8, pp. 4994–5007, Aug. 2013.

[11] E. García, J. A. Paredes, F. J. Álvarez, M. C. Pérez, and J. J. García, "Spreading sequences in active sensing: A review," *Signal Process.*, vol. 106, pp. 88–105, Jan. 2015.

[12] R. Feger, C. Wagner, S. Schuster, S. Scheiblhofer, H. Jager, and A. Stelzer, "A 77-GHz FMCW MIMO radar based on an SiGe single-chip transceiver," *IEEE Trans. Microw. Theory Techn.*, vol. 57, no. 5, pp. 1020–1035, May 2009.

[13] M. Farhadi, R. Feger, J. Fink, T. Wagner, and A. Stelzer, "Automotive synthetic aperture radar imaging using TDM-MIMO," in *Proc. IEEE Radar Conf. (RadarConf)*, May 2021, pp. 1–6.

[14] J. Bechter, F. Roos, and C. Waldschmidt, "Compensation of motion-induced phase errors in TDM MIMO radars," *IEEE Microw. Wireless Compon. Lett.*, vol. 27, no. 12, pp. 1164–1166, Dec. 2017.

[15] T. Dash, H. Driessen, O. A. Krasnov, and A. Yarovoy, "Counter-aliasing is better than de-aliasing: Application to Doppler weather radar with aperiodic pulse train," *IEEE Trans. Geosci. Remote Sens.*, vol. 62, 2024, Art. no. 5109017, doi: 10.1109/TGRS.2024.3438567.

[16] S. Yuan, F. Fioranelli, and A. Yarovoy, "High-resolution imaging algorithms for automotive radar: Challenges in real driving scenarios," *IEEE Aerosp. Electron. Syst. Mag.*, vol. 40, no. 7, pp. 30–43, Jul. 2025.

[17] F. Roos, J. Bechter, N. Appenrodt, J. Dickmann, and C. Waldschmidt, "Enhancement of Doppler unambiguity for chirp-sequence modulated TDM-MIMO radars," in *IEEE MTT-S Int. Microw. Symp. Dig.*, Apr. 2018, pp. 1–4.

[18] C. M. Schmid, R. Feger, C. Pfeffer, and A. Stelzer, "Motion compensation and efficient array design for TDMA FMCW MIMO radar systems," in *Proc. 6th Eur. Conf. Antennas Propag. (EUCAP)*, Mar. 2012, pp. 1746–1750.

[19] T. Dash, H. Driessen, O. A. Krasnov, and A. Yarovoy, "Doppler spectrum parameter estimation for weather radar echoes using a parametric semianalytical model," *IEEE Trans. Geosci. Remote Sens.*, vol. 62, 2024, Art. no. 5100218, doi: 10.1109/TGRS.2023.3338233.

[20] D. E. Goldberg, *Genetic Algorithms in Search, Optimization and Machine Learning*, 1st ed., Reading, MA, USA: Addison-Wesley, 1989.

[21] S. Kirkpatrick, C. D. Gelatt, and M. P. Vecchi, "Optimization by simulated annealing," *Science*, vol. 220, no. 4598, pp. 671–680, 1983.

[22] C. Audet and J. E. Dennis, "Analysis of generalized pattern searches," *SIAM J. Optim.*, vol. 13, no. 3, pp. 889–903, Jan. 2002.

[23] T. I. Inc. (2019). *Design Guide: Tidep-01012–Imaging Radar Using Cascaded mmWave Sensor Reference Design (Rev. A)*. [Online]. Available: https://www.ti.com/lit/ug/tiduen5a/tiduen5a.pdf

[24] S. Peleg and B. Porat, "The Cramèr–Rao lower bound for signals with constant amplitude and polynomial phase," *IEEE Trans. Signal Process.*, vol. 39, no. 3, pp. 749–752, Mar. 1991.

Sen Yuan (Member, IEEE) was born in Shanxi, China, in 1998. He received the Ph.D. degree in electrical engineering from Delft University of Technology, Delft, The Netherlands, in 2024.

He is currently a Post-Doctoral Researcher with the Group of Microwave Sensing, Signals and Systems (MS3), Delft University of Technology. His research interests include SAR imaging, signal processing for radar systems, and a new scheme of radar system design.

Dr. Yuan was a recipient of the European Microwave Association Student Grant in 2021, 2022, 2023, and 2024. He serves as an Associate Editor for *IEEE Aerospace and Electronic Systems Magazine* and an Associate Member of the IEEE Signal Processing Society Autonomous Systems Initiative (ASI).

Tworit Dash (Member, IEEE) was born in Odisha, India. He received the B.Tech. degree in instrumentation and electronics engineering from the College of Engineering and Technology, Bhubaneswar, India, in 2016, the M.Sc. degree (cum laude) in electrical engineering, specializing in telecommunication and sensing systems, from Delft University of Technology, Delft, The Netherlands in 2020, and the Ph.D. degree in radar signal processing with the Microwave Sensing, Signals, and Systems (MS3) Group, TU Delft, Delft, 2025.

Currently, he works as a Post-Doctoral Researcher, focusing on the formulation of electromagnetic inverse problems for *PHased Array Radar for Atmospheric Research* (PHARA) and the development of advanced signal-processing algorithms for atmospheric parameter retrieval.

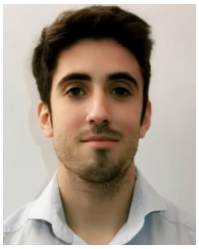

Ignacio Roldan received the B.Sc. and M.Sc. degrees in telecommunication engineering and the M.Sc. degree in signal processing and machine learning from the Universidad Politécnica de Madrid, Madrid, Spain, in 2014, 2016, and 2018, respectively, and the Ph.D. degree from Delft University of Technology, Delft, The Netherlands, in November 2024.

He worked for over five years at Advanced Radar Technologies, a Spanish Technology Company specializing in the design and manufacturing of radar systems. During this time, he contributed to several international projects, developing state-of-the-art signal-processing techniques for radar applications. In his final years at the company, he focused on applying machine learning techniques to UAV detection and classification. In September 2020, he joined the Microwave Sensing, Signals, and Systems group at Delft University of Technology. His research interests include automotive radar target detection using neural networks.

Dr. Roldan was awarded the Best Student Paper at the 2024 IEEE Radar Conference in Denver, USA.

Francesco Fioranelli (Senior Member, IEEE) received the Ph.D. degree from Durham University, Durham, U.K., in 2014.

He is currently an Associate Professor at TU Delft, Delft, The Netherlands. He was an Assistant Professor at the University of Glasgow, Glasgow, U.K., from 2016 to 2019, and a Research Associate at University College London, London, U.K., from 2014 to 2016. He has authored over 190 peer-reviewed publications, edited the books on *Micro-Doppler Radar and Its Applications* and *Radar Countermeasures for Unmanned Aerial Vehicles* (IET-Scitech, in 2020). His research interests include the development of radar systems and automatic classification for human signatures analysis in healthcare and security, drones and UAVs detection and classification, and automotive radar.

Dr. Fioranelli received four Best Paper Awards and the IEEE AESS Fred Nathanson Memorial Radar Award 2024.

Alexander G. Yarovoy (Fellow, IEEE) received the Diploma degree (Hons.) in radiophysics and electronics from Kharkov State University, Kharkiv, Ukraine, in 1984, and the Candidate Physics and Mathematical Science and Doctor Physics and Mathematical Sciences degrees in radiophysics from Kharkov State University, in 1987 and 1994, respectively.

In 1987, he joined the Department of Radiophysics, Kharkov State University, as a Researcher and became a Full Professor in 1997. From September 1994 to 1996, he was with the Technical University of Ilmenau, Ilmenau, Germany, as a Visiting Researcher. Since 1999, he has been with Delft University of Technology, Delft, The Netherlands, where he has been leading as the Chair of Microwave Sensing, Systems and Signals, since 2009. He has authored and co-authored more than 500 scientific or technical papers, seven patents, and 15 book chapters. His main research interests are in high-resolution radar, microwave imaging, and applied electromagnetics (in particular, UWB antennas).

Prof. Yarovoy was a recipient of the European Microwave Week Radar Award for the article that best advances the state-of-the-art in radar technology in 2001 (together with L.P. Ligthart and P. van Genderen) and in 2012 (together with T. Savelyev). In 2010, together with D. Caratelli, he got the Best Paper Award of the Applied Computational Electromagnetic Society (ACES). He served as the General TPC Chair of the 2020 European Microwave Week (EuMW'20), the Chair and the TPC Chair for the fifth European Radar Conference (EuRAD'08), as well as the Secretary of the first European Radar Conference (EuRAD'04). He also served as the Co-Chair and TPC Chair for the Tenth International Conference on GPR (GPR2004). He served as an Associated Editor of IEEE TRANSACTION ON RADAR SYSTEMS and the *International Journal of Microwave and Wireless Technologies* from 2011 to 2018. From 2008 to 2017, he served as the Director of the European Microwave Association (EuMA).